# Visualizing Compactifications for Outer Billiards on Quadratic Irrational Kites

John Hawley

May 3, 2012

# Contents

# 1 Introduction

A piecewise isometric map is a function on a metric space that divides the space into pieces and transforms them under maps that preserve distance. Polygonal outer billiards is a dynamical system arising from particular piecewise isometric maps taking a subset of the plane $\mathbb{R}^2$ to itself. To define this outer billiards map, choose a convex polygon $P$. For any point $(x_0, y_0)$ in $\mathbb{R}^2 - P$, its image $(x_1, y_1)$ under the outer billiards map is the unique point such that the line from $(x_0, y_0)$ to $(x_1, y_1)$ has a vertex of $P$ as its midpoint and any point in $P$ is to the left of this line. An illustration of this map when $P$ is a kite is shown in Figure 1.

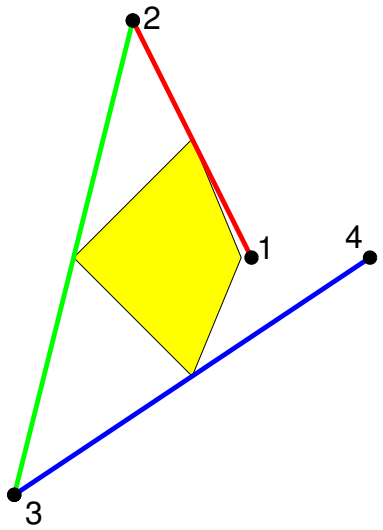


Figure 1: The outer billiards map relative to a kite

While there is currently no full description of the dynamics of the outer billiards map for general polygons, much is known about more specific cases. The boundedness of orbits and whether they are periodic are questions of particular interest. The works [6][2][1] showed that all outer billiard orbits for a special class of polygons called *quasi-rational* polygons are bounded; additionally, they showed that the subclass consisting of polygons with rational vertices has only periodic orbits. In [4], Tabachnikov demonstrated the existence of bounded aperiodic orbits for the regular pentagon (a quasi-rational, non-rational polygon). More recently, Schwartz in [3] gave a set of kites on which unbounded aperiodic orbits exist. The book [5] has a survey of other results about outer billiards.

One helpful way of analyzing outer billiards involves recognizing it as a polytope exchange map. A *polytope exchange* is a map from a subset of $\mathbb{R}^n$ into itself together with a lower-dimensional subspace. It divides the subset into polytope pieces and transforms them isometrically so that their collective image covers

the same $n$-volume as the domain. The lower-dimensional subspace allows the map to be undefined at the boundaries of the polytopes (where it can be ambiguous). On $\mathbb{R}$, $\mathbb{R}^2$, and $\mathbb{R}^3$, polytope exchanges are known as *interval exchanges*, *polygon exchanges*, and *polyhedron exchanges* respectively. Polytope exchanges are commonly required to be *locally finite*; that is, any bounded neighborhood in the domain contains only finitely many polytopes. Such exchange maps can have domains which are either compact (in which case they are comprised of a finite number of polygonal pieces) or not. The outer billiards map is an example of a locally-finite, non-compact polygon exchange map ([3]).

Although not much is known about general polygon exchange maps, compact polygon exchanges that move finitely many pieces are in some sense easier to analyze than non-compact exchanges. With only finitely many polygons to consider, it is possible to visualize the entire system and notice patterns therein. We can take advantage of this for non-compact systems if we can find a *compactification* for them. A compactification is an injection from the domain of a dynamical system into a compact domain that is also compatible with the dynamics. If $f : X \to X$ is the original function of interest, $i : X \to Y$ is an injection into a compact space $Y$, and $\hat{f} : Y \to Y$ is a map on the compact space, then this is a compactification if the square in Figure 2 communtes.

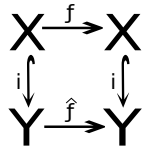


Figure 2: In a compactification, $i(f(x)) = \hat{f}(i(x))$ for all $x \in X$

Compactifications of the outer billiards map and related constructions have already proven useful. Schwartz in [3] presents and uses a compactification of a *first return map* (explained later) for the outer billiards map on kites. In this work, we give an algorithm for computing a related compactification of the outer billiards map on many members of the class of quadratic irrational kites (defined later) and show some pictures of the compactifications generated by the algorithm. While the images we produce are only numerical non-dense approximations of the actual compactification, we conjecture that our algorithm (with modifications) could be used to visualize the compactification for any parameter with any desired level of precision.

# 2 Background

## 2.1 The Outer Billiards Map

First, we will make precise our definition of the outer billiards map with respect to a kite. Let $K$ be a kite with vertices $(-1, 0), (0, -1), (0, 1)$, and $(A, 0)$ for $A > 0$. This parameter $A$ is an affine invariant of the kite; specifically, it is the

ratio of the areas cut off by the asymmetric diagonal (see Figure 3). That $A$ is an affine invariant is important because outer billiards is *affinely natural* in the following sense: the map is defined in terms of midpoints of line segments, so orbits are mapped to orbits under affine transformations.

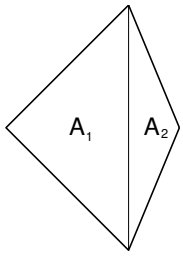


Figure 3: $\frac{A_2}{A_1} = A$ is an affine invariant for kites

Consider the set $R$ of four rays in $\mathbb{R}^2$ starting from the vertices labeled $I, II, III, IV$ (as shown in Figure 4).

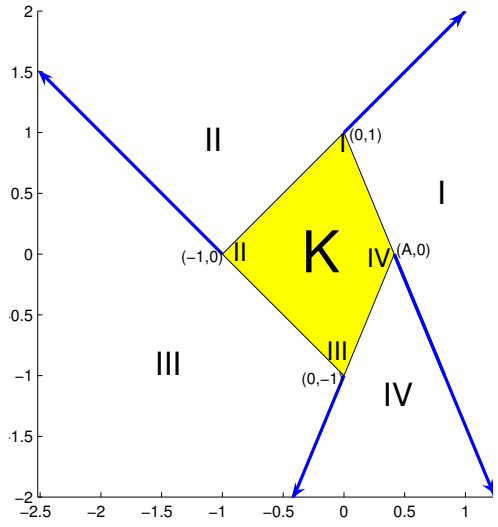


Figure 4: The regions that determine the outer billiards map relative to a kite

Now define a map

$$\phi : \mathbb{R}^2 - (K \cup R) \to \mathbb{R}^2 - K$$

such that a point in the region $I$ in Figure 4 is rotated by 180° around the vertex $I$, a point in $II$ is rotated by 180° around $II$, and so on. This is essentially the *outer billiards map*; however, this is not exactly the map we will analyze.

Notice that there are points whose images lie in $R$. For example, $\phi(A, A+1) = (A, -A-1) \in R$. To allow $\phi^n(x,y)$ to exist for any $n \in \mathbb{Z}$, define a new set

$$X = K \cup \left( \bigcup_{k=0}^{\infty} \left(\phi^{-1}\right)^k (R) \right)$$

This set is just $K$ together with a countable family of lines, so our function will be defined almost everywhere in $\mathbb{R}^2 - K$. We would also prefer to work with the map $\phi^2$ instead of our original map for computational reasons. From now on, we will refer to

$$\begin{aligned} \psi : \mathbb{R}^2 - X &\to \mathbb{R}^2 - X \\ (x,y) &\mapsto \phi^2(x,y) \end{aligned} \tag{1}$$

as the (squared) *outer billiards map*.

Now consider the set of lines

$$\mathbb{R} \times \mathbb{Z}_{odd} = \{(r, 2n+1) \mid r \in \mathbb{R}, n \in \mathbb{Z}\}.$$

One useful property of $\phi$ and $\psi$ is that, where they are defined, they map $\mathbb{R} \times \mathbb{Z}_{odd}$ into itself. The map $\phi$ is locally a rotation by $180^\circ$ about one of four points. Any such rotation can be decomposed as a translation mapping the center of rotation to the origin, a reflection about the origin, and the inverse translation. Expanding this decomposition of $\phi(x,y)$ for $(x,y) \in \mathbb{R} \times \mathbb{Z}_{odd}$ in each of the four regions, we see the following results:

$$\begin{array}{lccccccc} I: & (x,y) & \mapsto & (x, y-1) & \mapsto & (-x, 1-y) & \mapsto & (-x, 2-y) \\ II: & (x,y) & \mapsto & (x+1, y) & \mapsto & (-x-1, -y) & \mapsto & (-x-2, -y) \\ III: & (x,y) & \mapsto & (x, y+1) & \mapsto & (-x, -y-1) & \mapsto & (-x, -y-2) \\ IV: & (x,y) & \mapsto & (x-A, y) & \mapsto & (-x+A, -y) & \mapsto & (-x+2A, -y) \end{array} \tag{2}$$

In each case, the original point is mapped back under $\phi$ into $\mathbb{R} \times \mathbb{Z}_{odd}$. Because $\psi$ is $\phi^2$ where it is defined, this set of lines is also invariant under $\psi$.

## 2.2 The First Return Map

In order to analyze the (square) outer billiards map, we will use its *first return map* to a certain set. Consider a general discrete dynamical system $f : X \to X$ and a subset $A$ of $X$. Define the first return map $\Pi_A$ of $f$ to $A$ at a point $a \in A$ as $f^n(a)$ for the $n$ such that $f^n(a) \in A$ and $f^m(a) \notin A$ for any $0 < m < n$. Intuitively, $\Pi_A$ takes a point, repeatedly applies $f$ to it, and sees where it ends up when it first lands back in $A$. We can also relax the requirement that $A \subset X$ and define $\Pi_A$ only on $A \cap X$ as above.

In the remainder of this work, we will additionally be interested in the behavior of $\psi$ on the set

$$\Sigma = (\Sigma_+ \cup \Sigma_-) \cap (\mathbb{R}^2 - X)$$

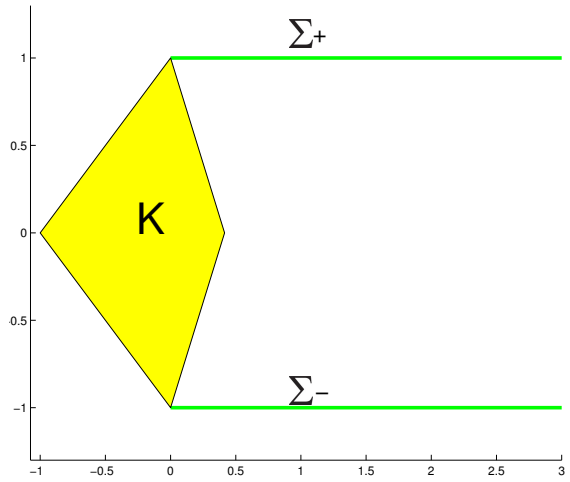


Figure 5: The sets $\Sigma_+$ and $\Sigma_-$

where $\Sigma_+ = \{(x, y) \mid y = 1 \text{ and } x > 0\}$ and $\Sigma_- = \{(x, y) \mid y = -1 \text{ and } x > 0\}$ as shown in Figure 5.

It remains to be seen that $\Pi_\Sigma$ is well-defined; that is, that points in $\Sigma$ eventually return to $\Sigma$ when we repeatedly apply $\psi$. The behavior of points in $\Sigma$ under $\psi$ far away from the kite is described in Section 2.3. This will establish that $\Pi_\Sigma$ is well-defined for most of $\Sigma$. Near the kite, it is much more difficult to prove that $\Pi_\Sigma$ is well-defined. Schwartz proves this result in [3] as part of the Pinwheel Lemma.

The compactification that we will generate pictures of will be a compactification of $\Pi_\Sigma$.

## 2.3 The Strips

In order to define our compactification of $\Pi_\Sigma$, we need to first define certain strips in the plane that factor significantly into the dynamics of $\psi$. These strips, exemplified by Figure 6, are determined by the parameter $A$. To generate each of the four strips, pick a side of the kite and extend it into a line. Reflect that line about the furthest vertex of the kite from the line so that this vertex is halfway between the two lines. The interior of these lines forms the strip. Strip $S_1$ is the region between the lines $y = -x - 1$ and $y = -x + 3$, strip $S_2$ is the region between $y = -\frac{1}{A}x + 1$ and $y = -\frac{1}{A}(x + 2 + A)$, and strip $S_3$ is the region between $y = \frac{1}{A}x - 1$ and $y = \frac{1}{A}(x + 2 + A)$. The fourth strip is the region between $y = x + 1$ and $y = x - 3$.

Sufficiently far away from the kite, the map $\psi$ exhibits regular behavior relative to these strips when applied to elements of $\Sigma$. A typical case is illustrated in Figure 7.

As can been in Figure 7, each point travels in a single direction until it

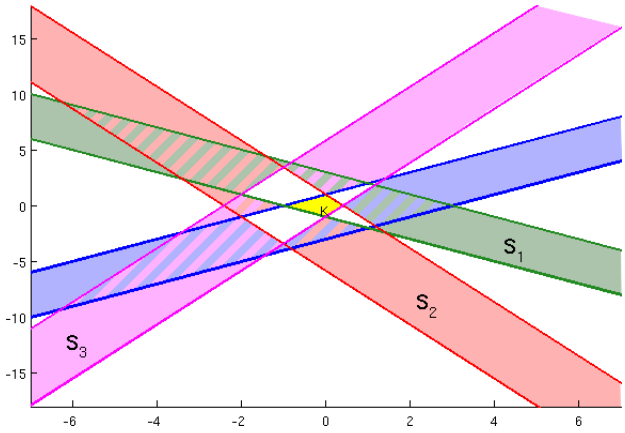


Figure 6: The strips $S_1$, $S_2$, and $S_3$ for $A = \sqrt{2} - 1$

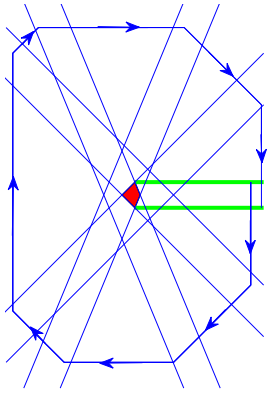

Figure 7: The behavior of $\psi$ far away from the kite

reaches the interior of a strip where it changes direction; this happens until the point returns to $\Sigma$. The demonstrated behavior is proven to occur for all points in $\Sigma$ that start sufficiently far from the kite as part of the proof of the Pinwheel Lemma in [3]. We will complete part of the necessary calculations to illustrate why this behavior exists. Suppose we have some point $(x, y)$ between the lines $y = -x + 3$ and $y = x - 3$ with $x \gg 0$ at which $\phi$ is well-defined. Per the diagram in Figure 4, $(x, y)$ will be in Region I. Equation 2 tells us that $\phi(x, y) = (-x, 2 - y)$. Because $x$ is large, $(-x, 2 - y)$ will lie in Region III. Equation 2 then says that $\phi(-x, 2 - y) = (x, y - 4)$. This means that $\psi(x, y) = (x, y) + (0, -4)$ for any $(x, y)$ satisfying the aforementioned conditions. Using this method, we could compute the seven other vectors like $(0, -4)$ that characterize this behavior of the squared outer billiards map.

### 2.4 The Compactification

Let $f_i(x,y)$ be the distance from the counterclockwise side of the strip $S_i$ to the point $\psi^n(x,y)$, where $n \in \mathbb{N}$ is the smallest iteration of $\psi$ such that $\psi^n(x,y)$ lies in $S_i$. This defines a map from $\Sigma$ to the interval $\left[0, 2\sqrt{2}\right]$ when $i = 1$ and $\left[0, \frac{2+2A}{\sqrt{1+A^2}}\right]$ otherwise. Let

$$\Lambda = \left[0, 2\sqrt{2}\right] \times \left[0, \frac{2+2A}{\sqrt{1+A^2}}\right] \times \left[0, \frac{2+2A}{\sqrt{1+A^2}}\right]$$

with the faces identified to form a 3-torus in the standard way. Our preliminary candidate map for the compactification is

$$\begin{aligned} f: \quad \Sigma \quad &\to \Lambda \\ (x,y) &\mapsto (f_1(x,y), f_2(x,y), f_3(x,y)) \,. \end{aligned}$$

In order to complete our definition of the compactification, we need to introduce a new restriction on our kite parameter $A$. When $A$ is in $(0,1)$ and quadratic irrational (i.e., $A \in \mathbb{Q}(\sqrt{D}) - \mathbb{Q}$ for squarefree $D$), the image of $\Sigma$ under $f$ is a non-dense embedding of a compact 2-torus in $\Lambda$; therefore, we henceforth restrict our attention to the case where $A$ is quadratic irrational. For ease of visualization, we will compose $f$ with a map $f(\Sigma) \to [0,1]^2$ that puts this 2-torus in the unit square with the standard identifications. Call this composition $f'$. This is the compactification of interest.

By the Master Picture Theorem in [3], $\Pi_\Sigma(x,y) - (x,y)$ can only be one of nine vectors if $(x,y) \in \Sigma_+$; they are

$$\begin{aligned} \{&(-2A-2, 0), (-2, -2), (2A-2, 0), (-2A, -2) \\ &(2A, -2), (2-2A, 0), (2, -2), (2A+2, 0), (0, 0)\}. \end{aligned} \tag{3}$$

Similarly, $\Pi_\Sigma(x,y) - (x,y)$ can only be one of nine vectors if $(x,y) \in \Sigma_-$. These vectors correspond to the vectors in (3) reflected about the origin. If we color the points $f'(x,y)$ in $f'(\Sigma)$ according to the vector $\Pi_\Sigma(x,y) - (x,y)$, we can see the behavior of $\Pi_\Sigma$ on the torus.

The construction of this compactification, while not identical to the one given in [3], has many similarities to it. There, the fact that $f(\Sigma)$ is a 2-torus embedded in a 3-torus follows naturally from the definition of the compactification. The map that is given there also commutes with the dynamics of the first return map. While we have no proof that the compactification we defined here has those same properties, it was true in all cases we tried that $f(\Sigma)$ was of dimension 2.

## 3 Method

The algorithm for drawing our approximation of the compactification $f'(\Sigma)$ can be broken down into four steps:

1. Compute the map $f$ of offsets into the strips
2. Assemble the embedded torus into a plane
3. Map the plane into the unit square
4. Compute the first return map and color each point

We begin by sampling a number of points from $\Sigma$. In our implementation of this algorithm, we sampled evenly-spaced points in $\Sigma$ starting at a small constant offset from $X$; however, we believe that randomly sampling would also produce good pictures.

## 3.1 Strip Offsets

For each sample point $(x, y)$, we start by computing $f_1(x, y)$, $f_2(x, y)$, and $f_3(x, y)$. For points close to the kite, we repeatedly compute the squared outer billiards map using the formulas in Equation 2 until we have the first entry points $(x_1, y_1)$, $(x_2, y_2)$, and $(x_3, y_3)$ into each of the strips $S_1$, $S_2$, and $S_3$ respectively. For points far away from the kite, we use the methods of Section 2.3 to precompute the vectors along which the iterations of $(x, y)$ under $\psi$ travel and compute $\psi$ using those. We then compute each $f_i$ as the distance from the counterclockwise-most strip. The distance functions are:

$$\begin{aligned} f_1(x, y) =& \frac{1}{\sqrt{2}}|x_1 + y_1 - 3| \\ f_2(x, y) =& \frac{1}{\sqrt{1 + A^2}}\,|x_2 + Ay_2 - A| \\ f_3(x, y) =& \frac{1}{\sqrt{1 + A^2}}\,|-x_3 + Ay_3 - A| \end{aligned}$$

## 3.2 Assembling the Plane

Once we have computed the strip maps, we can plot the resulting embedding of a 2-torus in $\Lambda$. This result is plotted in Figure 8.

The 2-torus manifests itself as some number of disjoint parallel planar subsets. By choosing a point in $f(\Sigma)$ and sorting the rest of the points by their distance from that point, we can efficiently get 3 non-colinear points in the same plane. This allows us to compute the normal vector $\vec{n} = (n_1, n_2, n_3)$ to all of the planes that appear.

For several reasons, we want to rotate all of the planes into a standard position. The rotation matrix $R$ that maps $\vec{n}$ to $(0, 0, 1)$ can be decomposed into two different axis-aligned rotations $R_z$ and $R_y$. Take

$$\theta_z = -\tan^{-1}\left(\frac{n_2}{n_1}\right),$$

$$\vec{n}' = (n_1', n_2', n_3') = R_z\vec{n},$$

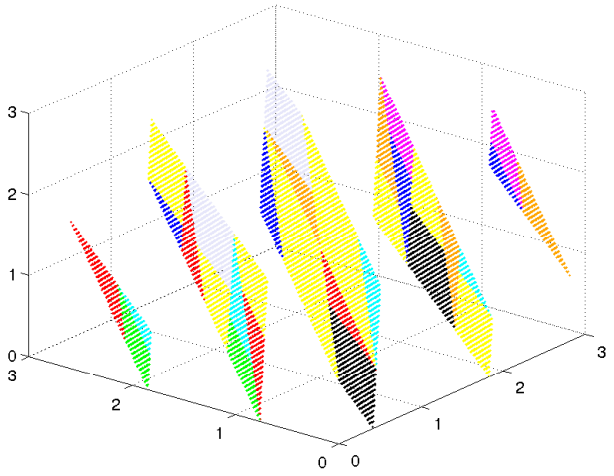


Figure 8: $f(\Sigma)$ embedded in $\Lambda$ for $A = \sqrt{2} - 1$

and

$$\theta_y = \tan^{-1}\left(\frac{n_3'}{n_1'}\right) - \frac{\pi}{2}.$$

Then

$$R_z = \begin{pmatrix} \cos(\theta_z) & -\sin(\theta_z) & 0 \\ \sin(\theta_z) & \cos(\theta_z) & 0 \\ 0 & 0 & 1 \end{pmatrix}, R_y = \begin{pmatrix} \cos(\theta_y) & 0 & \sin(\theta_y) \\ 0 & 1 & 0 \\ -\sin(\theta_y) & 0 & \cos(\theta_y) \end{pmatrix},$$

with $R = R_z R_y$.

By applying $R$ to the points in $f(\Sigma)$, we can count the number of distinct planes by counting the number of distinct heights. Call this count $N$.

What we describe next works for many $A$ but not all $A$. We align $N$ duplicates of $f(\Sigma)$ along the z-axis and compute the number of distinct planar subsets. Rotate these planes by $R$ and take the one of median height. In many cases, this will be a complete, correctly-glued copy of $f(\Sigma)$. Figure 9 shows a plot of the duplicates surrounding a complete copy of $f(\Sigma)$ for $A = \sqrt{5} - 2$ (a parameter for which $N = 4$). For a discussion of why this method fails for general $A$ and some possible alternatives, see Section 3.5.

## 3.3 Mapping the Plane to the Torus

Projecting the plane we produced above into $\mathbb{R}^2$, we obtain a parallelogram. This parallelogram can be easily mapped into the unit square via an affine transformation.

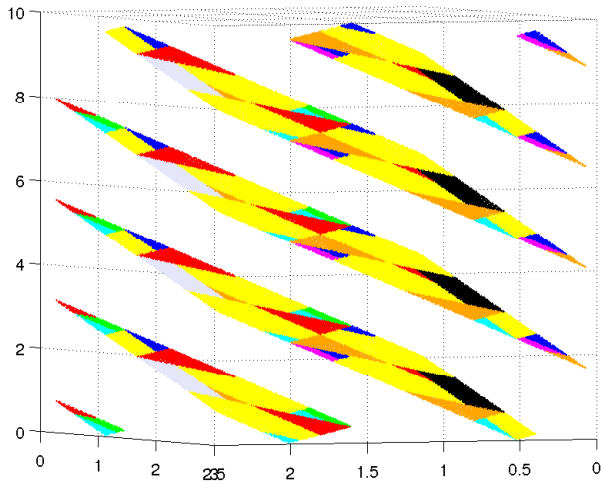


Figure 9: $N = 4$ copies of $f(\Sigma)$ for $A = \sqrt{5} - 2$

### 3.4 Coloring the Points

For each sample point $(x, y)$, we compute $\Pi_\Sigma(x, y)$ and color the point according to which vector $\Pi_\Sigma(x, y)$ is. Our computation of $\Pi_\Sigma$ takes advantage of the implications of the Pinwheel Lemma and follows the precomputed vectors and changing direction when a strip is hit.

### 3.5 Limitations

Some parameters $A$ for which we were able to generate a compactification include:

| | | | | |
|---|---|---|---|---|
| $\sqrt{2}-1$ | $\sqrt{3}-1$ | $\sqrt{5}-2$ | $\sqrt{6}-2$ | $\sqrt{7}-2$ |
| $2\sqrt{2}-2$ | $\sqrt{10}-3$ | $\sqrt{11}-3$ | $2\sqrt{3}-3$ | $\sqrt{13}-3$ |
| $\sqrt{14}-3$ | $\sqrt{19}-4$ | $2\sqrt{7}-5$ | $\sqrt{37}-6$ | $\sqrt{43}-6$ |
| $2\sqrt{14}-7$ | $\frac{\sqrt{2}}{2}$ | $\frac{\sqrt{13}}{5}$ | $\frac{\sqrt{2}-1}{2}$ | $\frac{\sqrt{3}-1}{2}$ |
| $\frac{\sqrt{5}-1}{2}$ | $\frac{\sqrt{17}-1}{4}$ | | | |

The main problem with the method proposed above is an implicit assumption we make about the structure of the embedding of the 2-torus. Figure 10 shows an embedded 2-torus for which our method does not work. As can be seen there, not all of the intermediate planar sections intersect both the $z = 0$ plane and the $z = \frac{2+2A}{\sqrt{1+A^2}}$ plane. This causes the reduplication method we outlined above to fail.

Another issue with this method is its space requirements. Duplicating $\Lambda$ using our current method requires $O(NS)$ space, where $N$ is the number of planes that appear and $S$ is the number of samples we take. Some of the

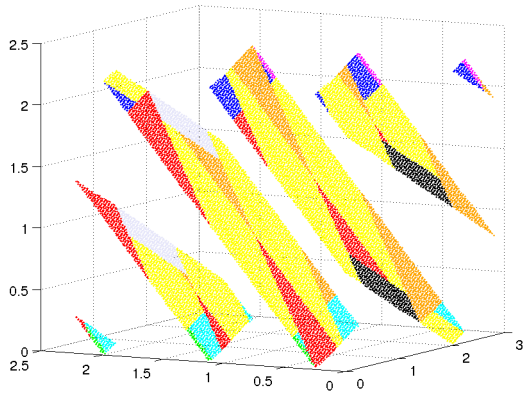


Figure 10: $f(\Sigma)$ for $A = \sqrt{17} - 4$

embedded 2-torii we examined were broken into as many as thousands of planes, and the number of samples required to get a good picture seemed to increase as the number of planes increases. This caused us to run out of memory when we tried to run the algorithm for some parameters.

We did some exploratory work on a different method for gluing the 2-torus back together which had some promising results. This alternate method involved finding the edges of the planar subsets and trying to glue edges of similar lengths. While we did not succeed in implementing a general version of this method, we did use it successfully to draw the compactification for $A = \sqrt{17} - 4$ (among others).

# 4 Results

Pictures generated for a variety of parameters $A$ are shown in Figures 11, 12, and 13.

In future work, we could attempt to analyze these pictures and characterize the polygons that appear in terms of the parameter $A$. We could also look at the induced action of the first return in hopes of finding a renormalization scheme for the polygon exchange map on the torus.

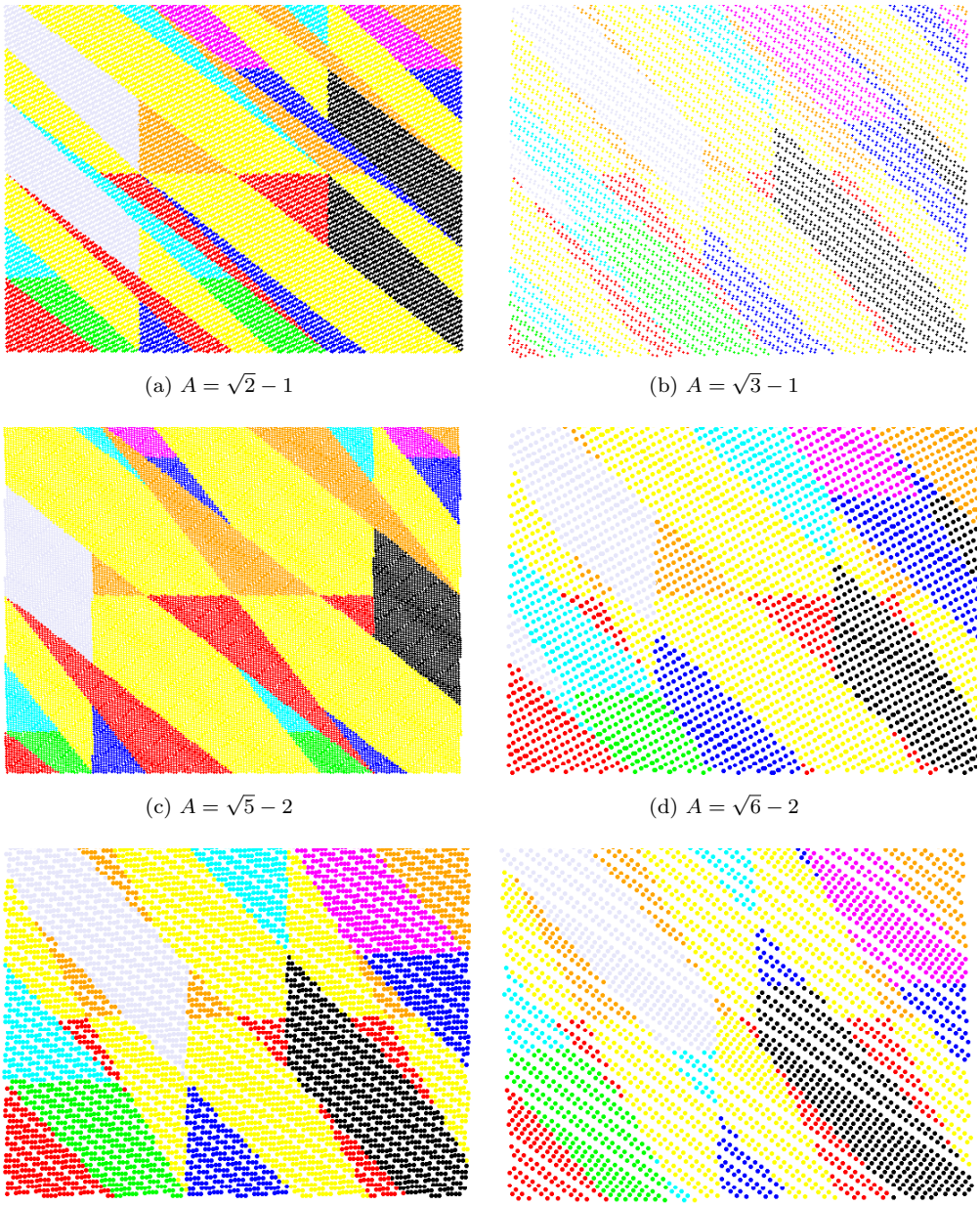

(a) $A = \sqrt{2} - 1$ (b) $A = \sqrt{3} - 1$

(c) $A = \sqrt{5} - 2$ (d) $A = \sqrt{6} - 2$

(e) $A = \sqrt{7} - 2$ (f) $A = 2\sqrt{2} - 2$

Figure 11: Pictures of the compactification for various parameters

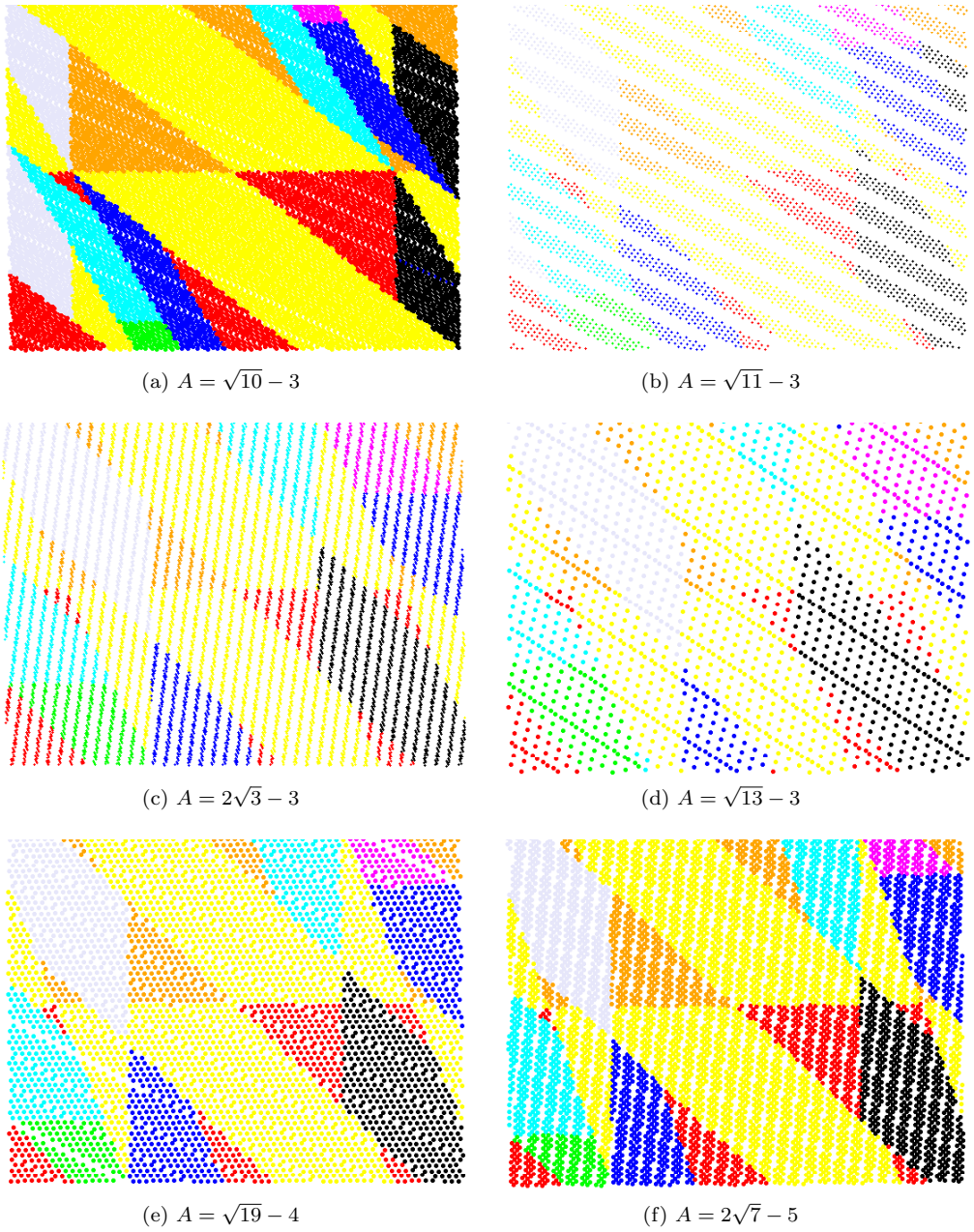

(a) $A = \sqrt{10} - 3$

(b) $A = \sqrt{11} - 3$

(c) $A = 2\sqrt{3} - 3$

(d) $A = \sqrt{13} - 3$

(e) $A = \sqrt{19} - 4$

(f) $A = 2\sqrt{7} - 5$

Figure 12: Pictures of the compactification for various parameters (continued)

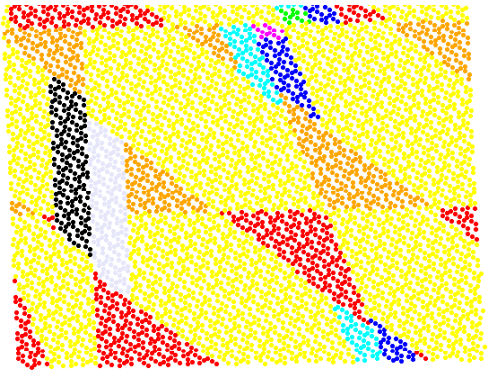

(a) $A = \sqrt{37} - 6$

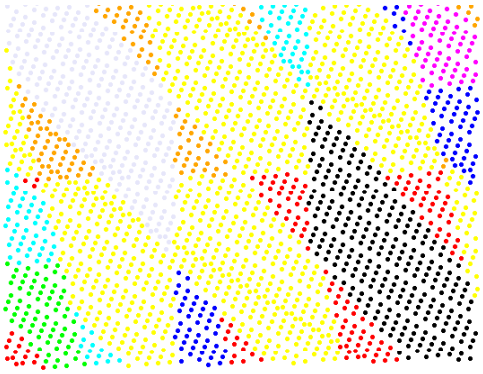

(b) $A = \sqrt{43} - 6$

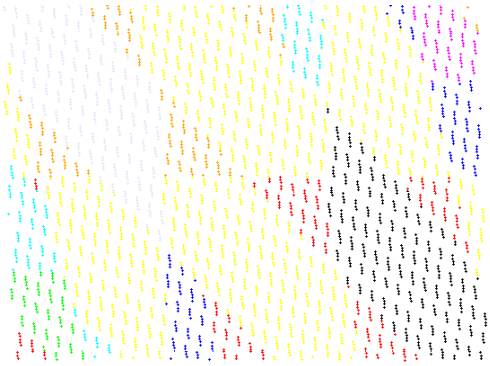

(c) $A = 2\sqrt{14} - 7$

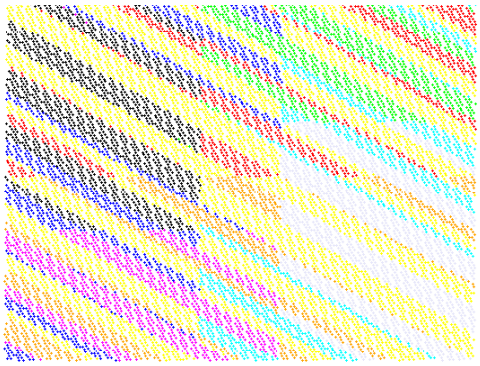

(d) $A = \frac{\sqrt{2}}{2}$

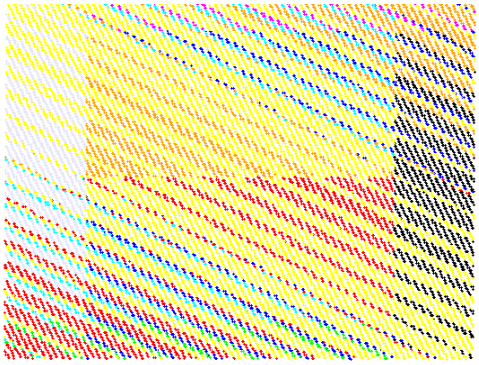

(e) $A = \frac{\sqrt{2}-1}{2}$

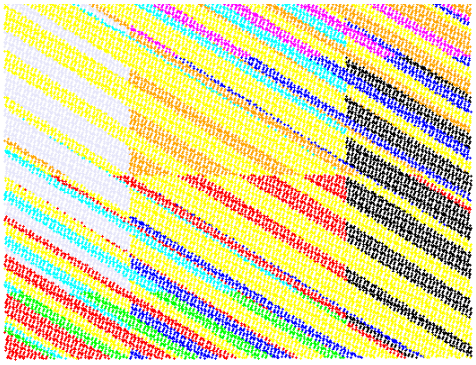

(f) $A = \frac{\sqrt{3}-1}{2}$

Figure 13: Pictures of the compactification for various parameters (continued)

# References


[1] E. Gutkin and N. Simanyi. Dual polygonal billiards and necklace dynamics. *Comm. Math. Phys.*, 143:431–449, 1992.

[2] R. Kolodziej. The antibilliard outside a polygon. *Bull. Polish Acad. Sci. Math*, 37:163–168, 1990.

[3] R. Schwartz. *Outer Billiards on Kites*. Princeton University Press, 2009.

[4] S. Tabachnikov. On the dual billiard problem. *Advances in Mathematics*, 115:221–249, 1995.

[5] S. Tabachnikov. *Geometry and Billiards*. American Mathematical Society, 2005.

[6] F. Vivaldi and A. Shaidenko. Global stability of a class of discontinuous dual billiards. *Comm. Math. Phys.*, 110:625–640, 1987.